Control of Variable-Speed Pumps Used as Turbines for Flexible Grid-Connected Power Generation

Thomas Mercier[a,b], Clément Hardy[a], Pierre Van Tichelen[a], Mathieu Olivier[b], Emmanuel De Jaeger[a]

[a]*Mechatronic, Electrical energy, and Dynamic Systems, Université catholique de Louvain, 1348, Louvain-la-Neuve, Belgium*

[b]*Department of Mechanical Engineering, Université Laval, G1V 0A6, Québec, QC, Canada*

Abstract

The increasing accommodation of intermittent renewable energies into power grids creates needs for additional flexibility in power generation. In the field of hydropower research, this has translated into significant attention paid to the larger control possibilities brought by power electronics converters. Through theoretical analysis and transient simulations, the present paper investigates the power control of a pump-as-turbine fed by a reservoir, and driving an induction machine, itself connected to the grid through a full-scale power converter. The modelling of each part of the system is thoroughly discussed and two control strategies are considered, namely the direct control of power through the electromagnetic torque, and the indirect control of power through the rotational speed. Theoretical analysis and transient simulations show that the first control strategy may lead to unstable operation, depending on the system and control parameters, while the second ensures the system stability.

Keywords: Hydraulic turbines, Hydroelectric power generation, Power generation control, Pump-as-turbine, Stability, Variable-speed drives.

Nomenclature

ω_m	Speed of rotor shaft
ϕ_{rd}	Rotor d-axis flux
ρ	Water density
ξ_s	Electrical angle between stator *Park* and α-β frames
A	Penstock cross section
f	Pipe friction factor, grid frequency
g	Acceleration due to gravity
H	Hydraulic head
i_{sd}, i_{sq}	d- and q-axis stator currents
L	Penstock length
L_{cr}, L_{cs}, L_m	Rotor, stator, and magnetising inductances
p	Number of pole pairs
P_{em}, P_{mec}	Electromagnetic and hydro-mechanical powers
Q	Water flow rate
u_{sd}, u_{sq}	d- and q-axis stator voltages
DFIM	Doubly-fed induction machine
FOC	Field oriented control
IM	Induction machine
PAT	Pump-as-turbine
VSI	Voltage source inverter

1. Introduction

Pumps used in reverse mode, i.e. as turbines (PATs, Pump-As-Turbines), are well known as an attractive solution for power generation in rural or remote areas [1, 2, 3, 4, 5], and for energy recovery in water distribution networks [6, 7, 8]. Compared to traditional hydraulic turbines, pumps are series-produced, available everywhere, cheaper, and easier to maintain. They are generally associated with an Induction Machine (IM) [9] and operated at a nearly fixed operation point. As only few pump manufacturers provide the characteristics of their machines in turbine mode, correlations are used to predict these from the pump mode characteristics [10, 11, 12].

☆https://doi.org/10.1016/j.epsr.2019.105962

Email address: thomas.mercier@uclouvain.be (Thomas Mercier[a,b])

In water distribution networks, PATs can be used instead of valves for pressure management, while recovering energy from the fluid. Research is then made to identify the best configurations of fixed- or variable-speed PATs and hydraulic valves [6, 7, 8].

Whether the application is power generation, or pressure management in water distribution systems, research on PATs has focused on their steady-state operation. Moreover, the use of a variable-speed drive, as in [6, 7], has only been considered in a high-level perspective, leaving control and stability considerations aside. The control and stability of hydraulic turbines is however not a new topic, historically focusing on fixed-speed machines equipped with guide vanes [13, 14].

In the last decades, developments in the fields of power electronics and power converters have brought new control possibilities to electrical machines, enabling to operate them at variable speed. In [15, 16, 17], the authors investigate the control of a variable-speed propeller turbine, driving a permanent magnet synchronous generator. The authors implement an adaptive maximum power point tracking, which constantly adjusts the rotational speed to match a varying flow-rate and maximize the turbine efficiency. None of [15, 16, 17] models the hydraulic dynamics.

Research is also made on the control of variable-speed Francis pump-turbines connected to a Doubly-Fed Induction Machine (DFIM) [18, 19, 20, 21], this time taking into account the hydraulic dynamics. In [18], the DFIM is fed by a three-level cascade as converter, and the authors show that power control dynamics is highest when power is controlled through the electromagnetic torque. Guide vanes are then adjusted to control speed and optimize the hydraulic efficiency. Reference [19] considers the control suggested in [18], and focuses on the governor tuning. The authors assume that the electromagnetic torque can instantaneously be controlled by the rotor-side inverter, reducing the DFIM model to a minimum and making abstraction of the control technique. Implementing the control recommendations made in [18], [20] simulates transients of the pump-turbine and DFIM, with a reduced-order versus detailed model for the hydraulic components of the overall system. In [21], the authors follow the recommendations of [18], and show that bigger steps in power setpoint can be carried out if the pump-turbine is connected to a synchronous machine with a full-scale power converter, instead of a DFIM with a partial-scale power converter.

The present paper bridges the gap between the research on PATs and the literature on the control and stability of hydraulic turbines. For the first time, it investigates the generation control of variable-speed machines without guide vanes, in this case PATs, taking the hydraulic dynamics and stability issues into account. Two control strategies are investigated, namely the direct control of power through the electromagnetic torque, as suggested in [18], and the indirect control of power through the rotational speed. The paper shows that the control strategy suggested in [18] may lead to rotational speed instability. The paper considers a specific configuration, which is introduced and whose modelling is thoroughly discussed in Section 2. The two control strategies and their stability are investigated in Section 3, and illustrated with simulation results in Section 4. Conclusions are given in Section 5.

Table 1: Overall characteristics of the considered power plant.

Penstock	Length	$L = 100$ m
	Section	$A = 0.099$ m^2
	Wave speed	$a = 364.18$ m/s
	Friction factor	$f = 0$
Pump	Power	$P_{BEP} = 10.85$ kW
	Rotational speed	$N_{BEP} = 985$ rpm
	Head	$H_{BEP} = 9.72$ m
	Flow rate	$Q_{BEP} = 343$ m^3/h
	Efficiency	$\eta_{BEP} = 83.67$ %
	Specific speed (m, m^3/s)	$N_S = 55.23$
	Wheel diameter	$D_{ref} = 0.296$ m
Induction machine	Rated apparent power	38.58 kVA
	Rated line voltage	400 V
	Frequency	50 Hz
	Number of poles pairs	3
	Moment of inertia	0.71916 kgm^2
Converter & grid connection	DC-link voltage	750 V
	DC-link capacitance	10 mF
	Filter inductances	1 mH
	Short circuit power	10 MVA

2. Characteristics and modelling of the considered power plant

The studied installation consists of a pump manufactured by *Ensival Moret*, which is used in turbine mode and fed by a reservoir whose water level varies from 5.9 to 9.75 meters. The PAT drives a three-phase IM connected to the grid through a reversible back-to-back power converter composed of two Voltage Source Inverters (VSI). The overall configuration is illustrated in Figure 1 and its main parameters are given in Table 1. Control strategies are tested on a model of the installation, which is developed in *Matlab-Simulink*, taking advantage of some already existing models of the *Simscape Power System* toolbox. The model is illustrated in Figure 2, and the following subsections discuss its main components: the water column, the hydraulic and electrical machines, and the grid connection.

2.1. Water column

The models generally used to study hydroelectric transients combine a model for the water column, with the characteristics of the considered hydraulic machine [13, 14]. Models for the water column can be of two types, commonly referred to as inelastic and elastic models. The former models an incompressible flow, while the latter takes into account the fluid compressibility and the pipe elasticity. The inelastic model can be described by a first-order differential equation [13, 14]:

$$\rho L \frac{dQ}{dt} = A\rho g \Delta H, \tag{1}$$

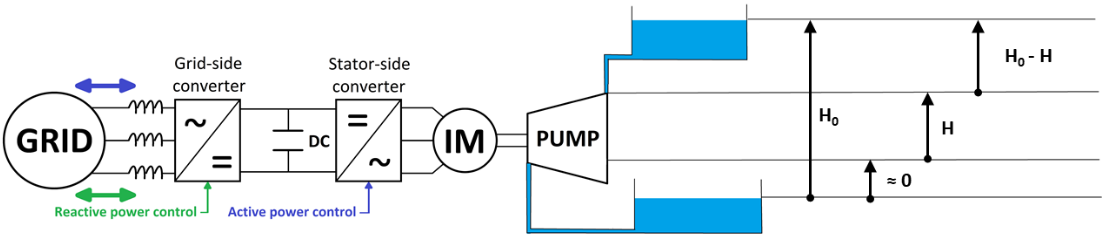

Figure 1: Electromechanical configuration of the studied power plant.

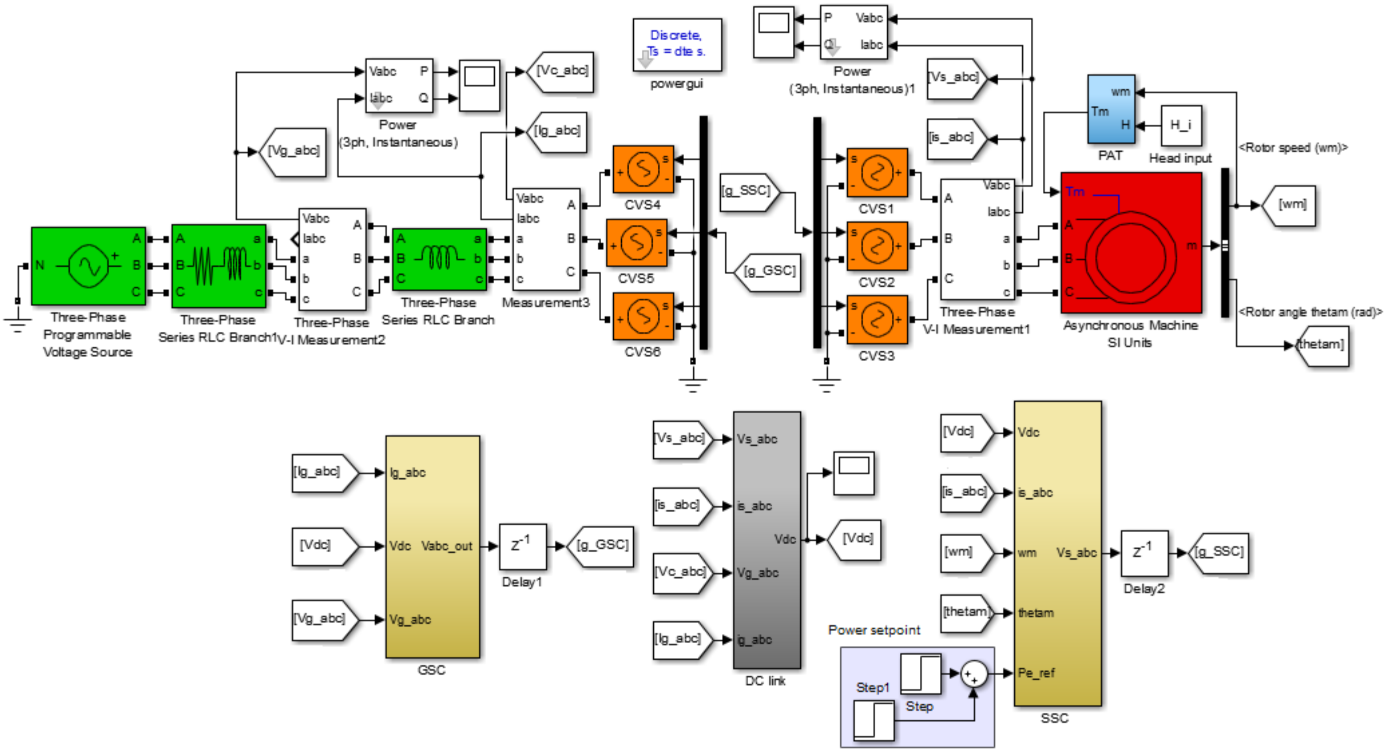

Figure 2: *Matlab-Simulink* model of the studied installation, with a PAT and a water column (blue), an IM (red), a power converter (orange) with its controls (yellow) and DC-link (grey), a grid connection (green). The two inputs are the head difference between the reservoirs, and the power setpoint.

with Q [m^3/s] the flow rate, L [m] the pipe length, A [m^2] its cross section, ρ [kg/m^3] the water mass density, g [m/s^2] the acceleration due to gravity and t [s] the time. The inelastic model is straightforward. The head at the upper reservoir varies slowly, and can therefore be considered constant, while the head at the turbine outlet is considered equal to the head at the lower reservoir[1]. As a consequence, varying guide vanes position or rotational speed induce pressure variations at the turbine inlet, i.e. non-zero ΔH [m] with the upper reservoir, which in turn make the flow rate adjust.

Elastic models of the water column enable to take into account pressure waves travelling back and forth in the pipe, as a result of changing operating conditions at the turbine level. The elastic model provides useful information for pipe design, e.g. the maximum pressure that may arise along the pipe as a result of hydraulic transients [22, 23]. Besides, it may also significantly refine simulation results of power output, as travelling pressure waves induce hydro-mechanical power oscillations which may be passed through to the electrical side. Compared to the inelastic model described by (1), the elastic model is more complex as it consists in a set of two partial derivative equations (PDEs) [13, 14, 24]:

$$\frac{\partial h}{\partial t} + \frac{a^2}{gA}\frac{\partial q}{\partial x} = 0, \tag{2}$$

$$\frac{\partial q}{\partial t} + gA\frac{\partial h}{\partial x} + \frac{fq\,|q|}{2DA} = 0, \tag{3}$$

with a [m/s] the wave velocity, f the friction factor, h and q the local head and flow rate. As explained in [24], the method of characteristics enables to transform this set of PDEs into a set of two ordinary differential equations (ODEs). The pipe is then spatially discretized and this set of two ODEs is solved for each pipe segment and at every simulation time step. Besides, for a non-zero friction factor ($f \neq 0$), the method of characteristics requires to solve a non-linear equation at each time step. Overall, the elastic model increases the computational cost. In the frame of the present paper, the friction factor is set to zero[2], as this choice does not affect the conclusions and enables a fair comparison of inelastic and elastic models. The two models were implemented in our overall model through *Matlab-Simulink* code and blocks, and they were tested on our case. As shown by simulation results of Section 4, they produce nearly identical results, while computational time is much higher[3] with the elastic model.

[1] The pipe segment connecting the hydraulic machine and the lower reservoir is generally neglected as it is usually one order of magnitude shorter than the other pipe segments.

[2] Typical values lie in the range 0.01 to 0.08, depending on pipe roughness and Reynolds number.

[3] In our case roughly one order of magnitude, although function of the model coding.

2.2. Dimensionless characteristics of the PAT

A quasi-steady assumption is generally used to characterise hydraulic machines in hydro-electric simulations. Considered characteristics are therefore non-dynamic, i.e. static, meaning that they do not consist in differential equations. Such characteristics can be represented through two classes of models. On the one hand, several models, linear or non-linear, have been developed for small to medium deviations around an operation point. These models approximate the characteristics by a simple analytic function calibrated at a given operation point [13, 14, 25, 26, 27]. The second class of models considers the machine detailed characteristics [15, 16, 17, 18, 21, 24], i.e. interpolation curves joining various operation points. The latter are suited for the study of large variations in operating conditions. Using the experimental correlations developed in [10], the characteristics in Figure 3a are obtained for the turbine mode operation of our studied pump. These are given using dimensionless numbers:

$$\phi = \frac{Q}{nD_{ref}^3}, \quad \psi = \frac{gH}{n^2D_{ref}^2} = f_1(\phi), \quad \pi = \frac{P_{mec}}{\rho n^3 D_{ref}^5} = f_2(\phi), \tag{4}$$

with hydro-mechanical power P_{mec} [W], rotational speed n [rps], and reference diameter D_{ref} [m], while the hydro-mechanical efficiency is defined as $\eta = \pi/\phi\psi = f_3(\phi)$. The PAT operation is characterized by one single parameter, the flow coefficient ϕ, while all other dimensionless numbers are metrics. Figure 3b shows the PAT operation range and the extent to which rotational speed variations enable power control. It is derived[4] from the PAT dimensionless characteristics, with as assumption the validity of similarity laws (geometric, kinematic and dynamic similarity). In practice, deviations from the predicted performances are observed as the PAT is operated further from its design rotational speed [28]. The effective PAT power range is then slightly different, e.g. narrower, from the one predicted through similarity laws. The discrepancies do however not affect the conclusions of the present paper.

The turbine mode characteristics are coded in *Matlab* and integrated in our overall model. The PAT sets head at its inlet, while the water column sets the flow-rate.

2.3. Electrical machine and grid connection

The pump depicted in Table 1 is coupled to a *W22 - Cast Iron Frame - High Efficiency - IE2* induction machine manufactured by *WEG*, which is modelled by the squirrel cage asynchronous machine of the *Simulink Simscape Power System* toolbox, neglecting saturation. Rotational speed is derived by the IM (red block, Figure 2) and fed to the PAT (blue block), which generates a torque signal feeding the IM.

[4] Given the PAT characteristics and reference diameter, setting values for ϕ and n enables to recover the head, flow rate, power and efficiency associated with each combination of ϕ and n.

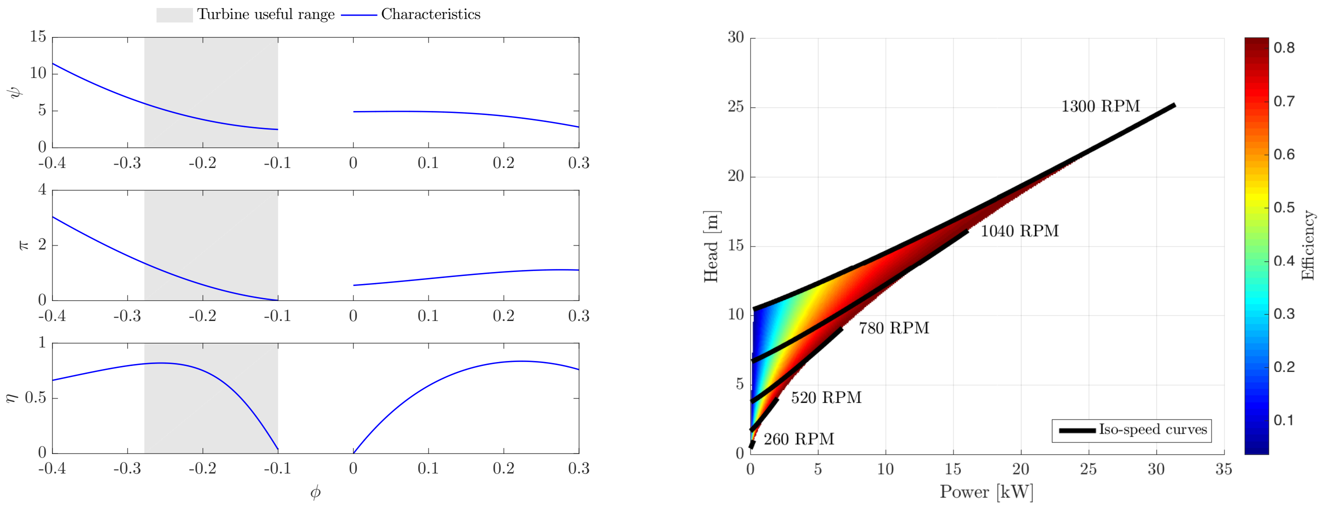

(a) Characteristics in turbine (left) and pump (right) modes.

(b) Turbine mode operation range, derived from the characteristics.

Figure 3: Characteristics and head versus power operation range of the studied PAT.

Table 2: Parameters used for the tuning of stator- and grid-side PI controllers. The stator-side outer loop is only used for the control of power through rotational speed.

	Stator-side VSI		Grid-side VSI	
	Outer loop	Inner loop	Outer loop	Inner loop
Nat. freq.	5 Hz	50 Hz	50 Hz	500 Hz
Damping	0.8	1	0.8	1

Regarding the power converter, there exists two main modelling philosophies, these are the so-called "detailed" and "average" models. Detailed models reproduce the switching dynamics of the converter semiconductors, thereby rendering the resulting high-frequency components in electrical quantities. Detailed models considerably increase computational time, while not significantly impacting hydraulic transients, the electrical dynamics being much faster [18]. Instead of the detailed model, we consider an average, also known as pseudocontinuous [18], lossless model for each of the two VSIs. The average model considers VSIs as controlled voltage sources, as understood in the classical electrical circuits theory, with reference voltages generated by the controls. The parameters used for the tuning the converters' proportional integral (PI) controllers are given in Table 2.

Our model includes a phase-locked loop and controlled voltage sources of the *Simulink Simscape Power System* toolbox (orange blocks, Figure 2), while the DC-link capacitor is implemented with *Simulink* elements (grey block, Figure 2). Filter inductors are used as an interface between the converter and the grid, and the latter is modelled through a *Thevenin* equivalent (green blocks, Figure 2). The considered filter inductances and short circuit power are given in Table 1.

2.4. Verification of the model

The overall model was built step by step, with verification phases at each of these steps. First, the control of the the IM and its feeding VSI were implemented. Verification was made that rotational speed and torque references can be followed, and that the IM nominal values can be reached without overshooting. The implementation of the grid-side VSI and its control were then carried out. It was checked that the DC-link voltage is kept at its nominal value, and that reactive power injections are regulated to support the grid voltage. The development of the PAT and water column were carried out aside from the electrical components. The extrapolated characteristics in turbine mode were compared with the measured characteristics in [10] for consistency check. The inelastic water column was then developed and linked to the PAT model. Arbitrary steps in rotational speed were imposed to the model to check the consistency of the resulting head and flow rate variations. The elastic model was then developed, and it was checked that it introduces pressure waves not accounted for by the inelastic model. The various submodels were finally coupled together, and the power control capability of the overall system was checked.

3. Power control strategies

The control of the overall installation is achieved through the two VSIs. On the one hand, based on vector control and the phase-locked loop of the *Simulink Simscape Power System* toolbox, the grid-side VSI keeps the DC-link voltage to its nominal value and regulate reactive power injections proportionally to grid-voltage deviations (Figure 4a). On the other hand, the control of the PAT power output is achieved through the stator-side VSI. This control is made of an inner loop based on Field-Oriented

Control (FOC), and an outer loop for which two strategies are considered: (i) the direct control of power through the electromagnetic torque, and (ii) the indirect control of power through the rotational speed. These strategies are illustrated in Figure 4b and thoroughly discussed in the following subsections, along with their stability. The focus is on the control strategy, rather than on the specific technique used to implement it, which might be FOC, Direct Torque Control[5], or any other technique such as neural networks and fuzzy logic controllers [29].

3.1. Control through the electromagnetic torque

Based on a power reference and an online measurement of rotational speed, a torque reference is defined, and followed in a matter of milliseconds given the fast electrical dynamics. However, inappropriate hydro-mechanical torque follow-up would translate into a torque unbalance, inducing a rotational speed deviation which may transform into an instability. It must therefore be checked that this control strategy does not lead to rotational speed instability.

3.1.1. Analysis of rotational speed stability

A theoretical stability condition is derived from reasoning on the balance of electromagnetic and electromechanical powers. Given the control strategy, the electromagnetic power P_{em} is firmly kept to its setpoint, even in case of infinitesimal speed deviation, so that we have

$$\frac{1}{P_{em}}\frac{dP_{em}}{dt} = 0. \tag{5}$$

On the hydro-mechanical side, a deviation in rotational speed instantaneously translates into variations in head, in PAT operation point and in hydro-mechanical power. A flow rate variation only occurs afterwards and progressively, as a result of the head variation, and translates into a hydro-mechanical power variation. The hydro-mechanical power dynamics can be studied based on the PAT characteristics as

$$P_{mec}(\phi, n) = \pi(\phi)\rho n^3 D_{ref}^5. \tag{6}$$

Using the chain rule to compute the derivative gives

$$\frac{1}{P_{mec}}\frac{dP_{mec}}{dt} = \frac{1}{\pi(\phi)}\frac{d\pi(\phi)}{d\phi}\left(\frac{\partial\phi}{dn}\frac{dn}{dt} + \frac{\partial\phi}{dQ}\frac{dQ}{dt}\right) + \frac{3}{n}\frac{dn}{dt}, \tag{7}$$

which, substituting (1) for the flow-rate dynamics, gives

$$\frac{1}{P_{mec}}\frac{dP_{mec}}{dt} = -\frac{1}{n}\frac{dn}{dt}\left(\frac{d\pi}{d\phi}\frac{\phi}{\pi} - 3\right) + \frac{d\pi}{d\phi}\frac{Ag\,(H-H_0)}{\pi n L D_{ref}^3}. \tag{8}$$

As shown by (8), the hydro-mechanical power dynamics is the sum of two terms. The first term is proportional to the speed dynamics, with a coefficient function of the PAT operation point, while the second term is function of both the PAT operation point and the water column parameters. The first term represents the hydro-mechanical power response to a variation in rotational speed, while the second term represents the response to a flow rate variation. We consider the simplifying case where the ratio of the penstock length to cross-section area, L/A, tends towards infinity. Given the lossless model of the water column, this assumption does not prevent a flow from occurring. Instead, as emphasized by (1), it makes the flow-rate adjust at an infinitely slow rate, i.e. the flow-rate is approximately constant, and (8) becomes

$$\frac{1}{P_{mec}}\frac{dP_{mec}}{dt} = -\frac{1}{n}\frac{dn}{dt}\left(\frac{d\pi}{d\phi}\frac{\phi}{\pi} - 3\right). \tag{9}$$

Given an initial steady operation point where both hydro-mechanical and electromagnetic powers are equal, and where the electromagnetic power is kept constant by the control (5), steady-state stability is ensured if the hydro-mechanical power increases ($P_{mec} < 0$, $dP_{mec}/dt \leq 0$) as rotational speed decreases ($n < 0$, $dn/dt > 0$), and inversely. This is the case whenever

$$\left(\frac{d\pi}{d\phi}\frac{\phi}{\pi} - 3\right) \geq 0. \tag{10}$$

This stability condition is only function of the PAT characteristics, and is in our case satisfied when $\phi \geq -0.19$ holds, which, as illustrated in Figure 3a, corresponds to the PAT low power and low efficiency range. The performed analysis puts in light that the direct control of power through the electromagnetic torque results in an unstable behaviour in most of the machine operation range. It should be noted that, although the threshold ϕ is affected by the accuracy of the characteristics, the qualitative result that there exists a stability limit holds no matter the accuracy of the characteristics. The stability limit and its form, as derived here above, are valid in the context of the assumptions made, which are that the water column is lossless and accurately modelled by (1), and that the PAT is fed through a water column whose ratio L/A tends towards infinity. As it is shown further in this paper, removing the assumption of infinite L/A ratio does however not prevent the instability.

The rotational speed instability can be illustrated with the simple *Simulink* model in Figure 5a. This model is a simplified version of our complete model, as it considers an instantaneous response of the electrical system, and a constant flow rate. This simplified model is run from several initial ϕ values, with power references, flow rates and rotational speeds initialized so that the system is nearly in steady-state. A 1% mismatch in rotational speed is introduced as a trigger of the rotational speed instabil-

[5]Direct torque control should not be confounded with the direct control of power through electromagnetic torque, which is a concept developed subsequently in the paper.

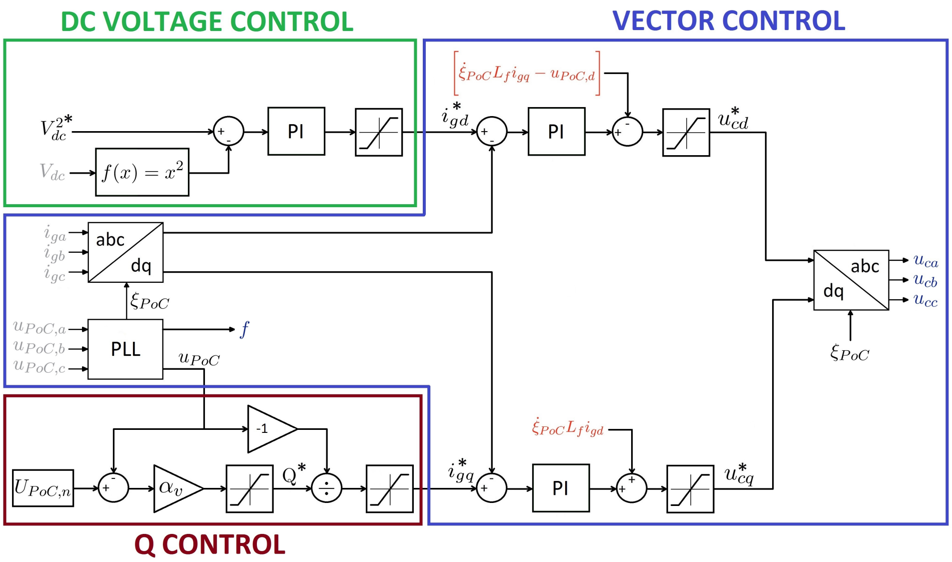

(a) Control of the grid-side VSI: the DC-link and grid voltages are controlled through active and reactive power injections.

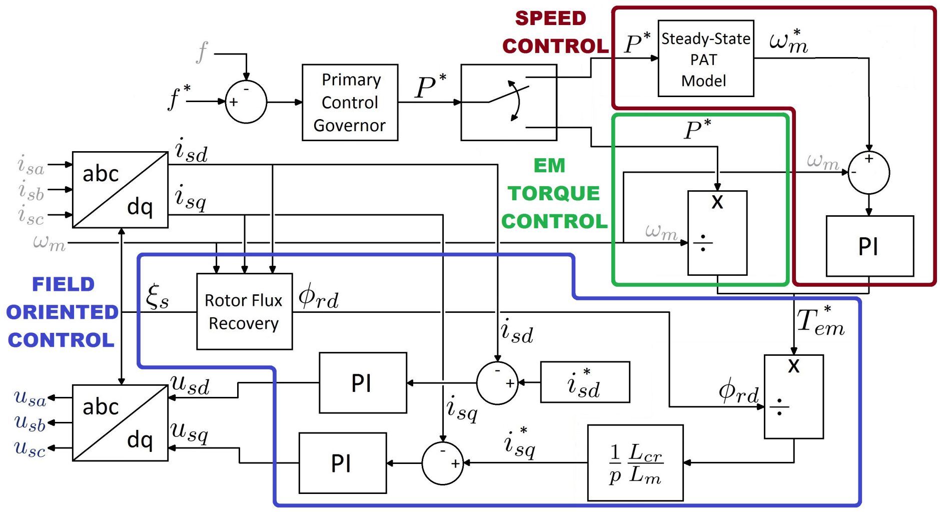

(b) Control of the stator-side VSI wih the two discussed strategies (in green and red), and a common inner FOC loop (in blue).

Figure 4: Block diagrams illustrating the control of the two VSIs. Asterisk superscripts denote setpoint signals and grey symbols refer to measured quantities.

ity. As shown in Figure 5b, the results obtained from this simple model show that the rotational speed collapses for $\phi < -0.19$. The same instability is observed with the complete model.

In practice, the ratio L/A may be large but is always finite. Removing the previous assumption, the head drop resulting from a decrease in rotational speed makes the flow-rate adjust, thereby increasing the hydro-mechanical power response. Given an operation point where the stability condition is not met, a positive flow rate adjustment rate might be such that the resulting hydro-mechanical power response is positive. The stability criterion is therefore sufficient to ensure the steady-state stability of the system, but it is neither necessary nor sufficient to ensure the transient stability, e.g. the system stability to a step increase in power setpoint. The system stability cannot be assessed with a simple criterion, but rather through many time-consuming transient simulations, as is done in [21] for a classical Francis turbine. As doing such simulations for a power plant of only a few kilowatts might not be feasible, the considered control strategy is discarded and a second control strategy is investigated.

3.1.2. Formal procedures of stability analysis

In order to study a system's stability, it is common to make the distinction between the standard frameworks of small-signal stability, and transient stability. The analysis carried out here above can be related to both. Based on the linearised expression of the rotational speed in the Laplace domain, $\Delta n(s)$, it can be shown that small-signal stability is achieved with (10) as a required and sufficient condition. In other words, (10) is a required and sufficient condition for the poles of $\Delta n(s)$ to lie in the left-hand side of the complex plane.

Compared to its small-signal counterpart, a system's transient stability is more difficult to assess. In the present work, transient stability is discussed and illustrated with time-domain simulations. More formal procedures exist to assess transient stability, e.g. Lyapunov-based approches [30, 31]. These are however considered out of the scope of the present paper and left for future work.

3.2. Control through the rotational speed

A natural strategy to overcome the instability discussed in Section 3.1 is to use the stator-side VSI to control the PAT rotational speed. Given a PAT characteristics and a water level, it is possible to map steady-state rotational speed and hydro-mechanical power. In the proposed control strategy, a rotational speed setpoint is thus defined based on a power setpoint, so that when the speed reaches its setpoint, and when hydraulic transients are completed, the generated power is equal to the power setpoint. During the transient, the generated power is not equal to its setpoint, and stability is thus achieved at the cost of transient precision in power control.

4. Simulation results

The overall model of the installation involves various time constants. On the hydraulic side, the inelastic water column time constant is $T_w = LQ_0/AgH_0 \approx 1$ [s], while the time required for pressure waves to travel the water column is $L/a = 0.27$ [s]. On the electrical side, the shortest time constant is associated with the inner control loop of the grid-side VSI, and is equal to $1/500 = 0.002$ [s] following design parameters. The time constant associated with the rotating masses is obviously much larger than the preceding value, and the most restricting is thus the electrical time constant. As a consequence, the various dynamics associated with the model should appropriately be captured with a 100 [μs] time-step. All the simulations are carried out with this fixed simulation time-step, and with *Simulink*'s implementation of the *Bogacki-Shampine* numerical scheme, which is an explicit *Runge-Kutta* method of order 3. The time step and numerical scheme were validated by running the most demanding case with a 25 [μs] time-step. Normalized differences in steady-state values of the quantities of interest were all below the 10^{-4} threshold. Regarding the simulated cases, the two investigated control strategies are tested when power steps and ramps, are applied to the system. This leads to a total of four simulated cases, which are illustrated by the results in Figure 6. Each of the four cases is run twice, respectively with the inelastic and elastic models of the water column. For each of the four cases, a decrease in power setpoint is imposed at $t = 5$ [s], from -7 [kW] to -0.7 [kW], followed by a power increase at $t = 25$ [s], from -0.7 [kW] to 7 [kW].

4.1. Control through the electromagnetic torque

The instability discussed in Section 3.1 is illustrated in Figure 6a. At $t = 5$ [s], the system reacts precisely and quickly to the step decrease in power setpoint. However, at $t = 25$ [s], the power increase leads to a collapse of the rotational speed. While the electromagnetic torque is adjusted rapidly to follow the power setpoint, the resulting flow rate adjustment is too slow to complete before the rotational speed reaches zero. The observed instability can be avoided if, instead of power steps, power ramps are imposed to the system. This is illustrated in Figure 6c. At $t = 25$ [s], the power ramp makes the rotational speed slide more slowly towards zero, leaving time for the flow rate to adjust. However, the ramp does not ensure the system stability to other transients of different magnitudes and from different initial operation point. Besides, deriving the maximum acceptable ramp rate would require a full simulation campaign, similar to what is done in [21], testing many step magnitudes and initial operation points. This is not conceivable for a small system as the one studied in the present paper. Another option to avoid the instability is to increase the inertia of rotating masses. Increased inertia would make the rotational speed slide toward zero at a lower pace, leaving time for the flow rate to adjust.

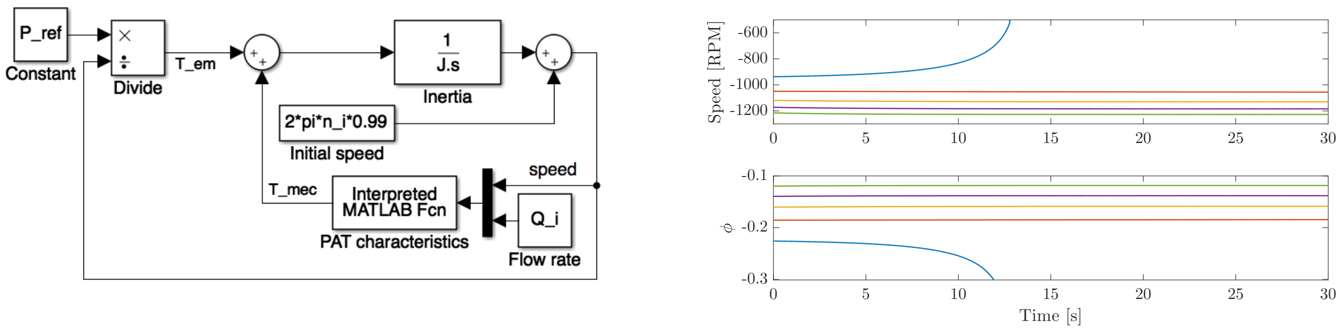

(a) Simplified *Simulink* model.

(b) Rotational speed collapses for $\phi < -0.19$.

Figure 5: Simplified *Simulink* model and simulation results illustrating the instability limit.

As for the ramp, this solution is not trivial to design and another control scheme is preferred.

4.2. Control through the rotational speed

By its very nature, the indirect control of power through rotational speed removes the potential instability. Indeed, as rotational speed is set by the controller, it is unable to collapse. Figure 6b illustrates the behaviour of the system with this control strategy and when a step in power setpoint is imposed to the system. The rotational speed is quickly and precisely adjusted as the power setpoint varies. In the meantime, and after rotational speed is set, the flow rate has all the required time to adjust, thereby ensuring the system stability. However, although stability is achieved, large undesired excursions of power are observed at $t = 5$ [s] and $t = 25$ [s]. These are induced by the shift of electromagnetic torque to its nominal value, following the change in rotational speed setpoint. Two options are available to avoid the large power excursions. Either the speed loop natural frequency can be decreased, or the step in power setpoint can be smoothed to a ramp. The first option is discarded, as it would leave the system more vulnerable to instabilities. Indeed, the speed control dynamics must remain faster than the hydraulic dynamics to ensure the system stability. The second option is implemented and illustrated by the results in Figure 6d. These results are similar to those observed in Figure 6c for the direct control of power with a rate limiter. There is however a major difference as, contrary to the direct control of power through electromagnetic torque, the indirect control of power through rotational speed remains stable even in case of bad design of the ramp rate.

5. Conclusions

Hydropower transients are characterised by various dynamics. In term of time scales, the electrical dynamics is the fastest, followed by the dynamics of rotating masses, and finally, the hydraulic dynamics is the slowest. The hydraulic dynamics is function of both the PAT characteristics and the parameters of the water column. Through theoretical analysis and transient simulations, the present paper shows that a too-demanding control strategy, in this case, the proposed direct control of power through the electromagnetic torque suggested in [18], might be unstable if it is not consistent with the hydraulic dynamics. To overcome the potential instability, either an extensive transient simulation campaign has to be carried out to validate the control strategy and its parameters, or a more robust control strategy should be considered. The present paper proposes a more robust control strategy, consisting in the indirect control of power through rotational speed. Stability is then ensured, but smooth power setpoint variations are required to avoid large transient power excursions. If a fast power control dynamics is required, increasing the inertia of rotating masses could avoid potential instabilities, though at the cost of a validating simulation campaign.

In the present paper, the subject of rotational speed stability is addressed through discussion, elementary mathematical developments and time-domain simulation results. Future work might consider more formal and well established procedures to assess stability.

Acknowledgment

The paper was made in the frame of *SmartWater*, a research project supported by the Walloon Region, Belgium.

References

[1] M. Binama, W.-T. Su, X.-B. Li, F.-C. Li, X.-Z. Wei, S. An, Investigation on pump as turbine (PAT) technical aspects for micro hydropower schemes: A state-of-the-art review, Renewable and Sustainable Energy Reviews 79 (2017) 148 – 179. `doi:10.1016/j.rser.2017.04.071`.

[2] A. Carravetta, S. D. Houreh, H. M. Ramos, Pumps as Turbines: Fundamentals and Applications, Springer, 2017. `doi:10.1007/978-3-319-67507-7`.

[3] S. V. Jain, R. N. Patel, Investigations on pump running in turbine mode: a review of the state-of-the-art, Renewable and Sustainable Energy Reviews 30 (2014) 841–868. `doi:10.1016/j.rser.2013.11.030`.

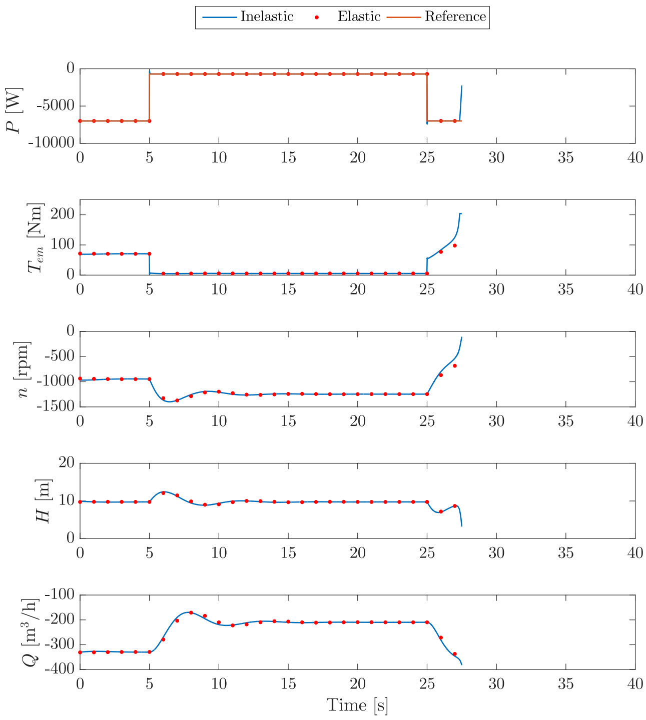

(a) Direct control of power, without power setpoint rate limiter.

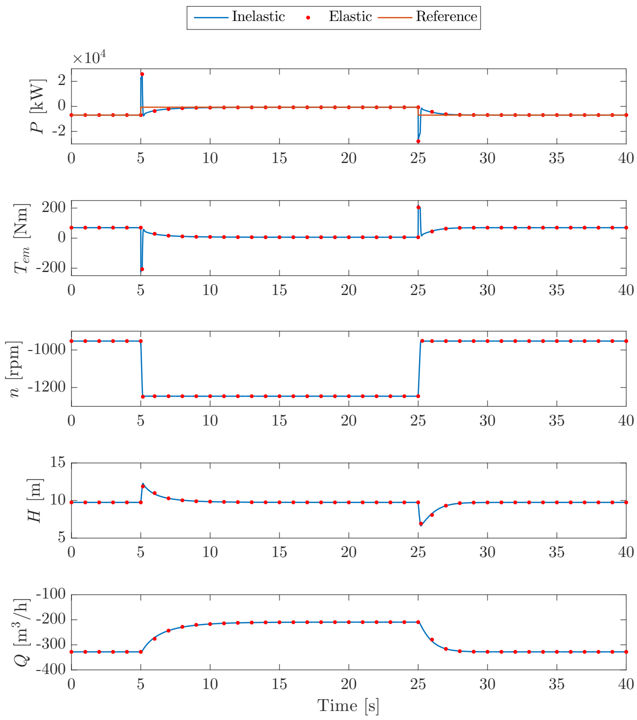

(b) Indirect control of power, without power setpoint rate limiter.

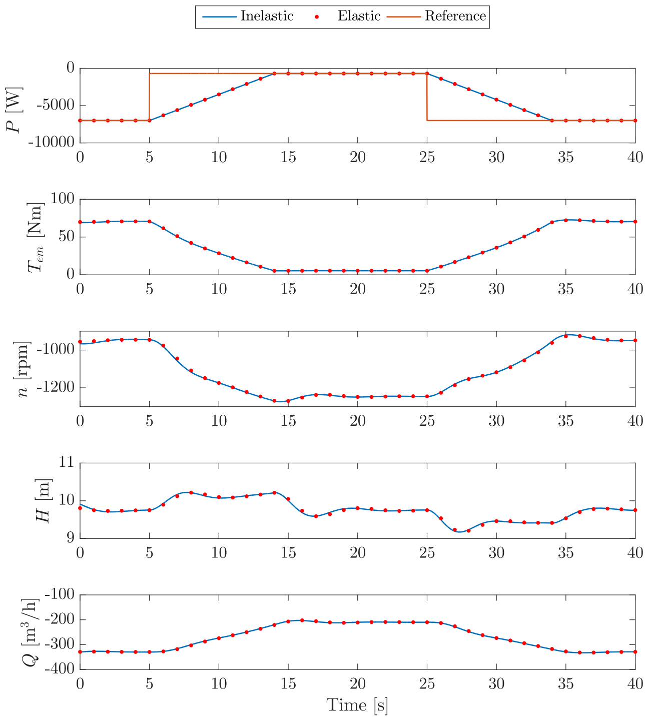

(c) Direct control of power, with power setpoint rate limiter.

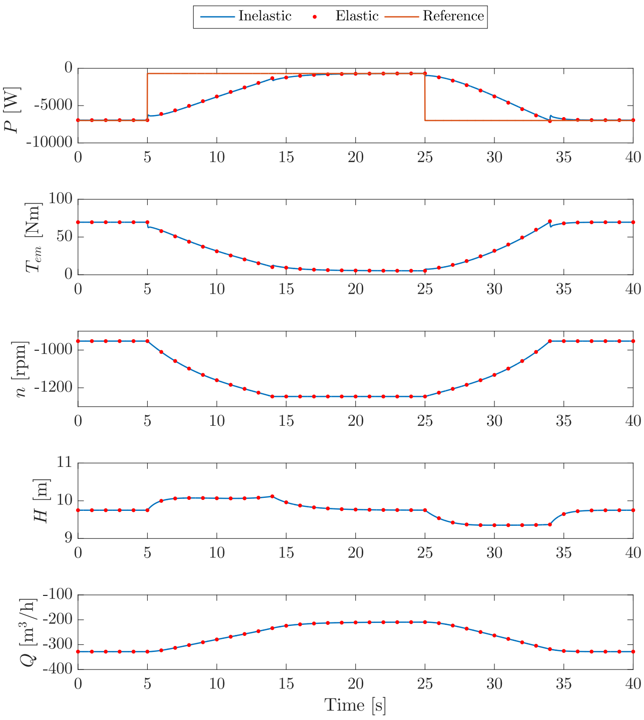

(d) Indirect control of power, with power setpoint rate limiter.

Figure 6: Simulation results illustrating the direct and indirect control of power through respectively electromagnetic torque and rotational speed. The figure shows the evolution of the different metrics (P_{mec}, T_{em}, n, H and Q) as a function of time.

[4] A. Elbatran, O. Yaakob, Y. M. Ahmed, H. Shabara, Operation, performance and economic analysis of low head micro-hydropower turbines for rural and remote areas: a review, Renewable and Sustainable Energy Reviews 43 (2015) 40–50. doi:10.1016/j.rser.2014.11.045.

[5] J. Laghari, H. Mokhlis, A. Bakar, H. Mohammad, A comprehensive overview of new designs in the hydraulic, electrical equipments and controllers of mini hydro power plants making it cost effective technology, Renewable and Sustainable Energy Reviews 20 (2013) 279–293. doi:10.1016/j.rser.2012.12.002.

[6] A. Carravetta, G. del Giudice, O. Fecarotta, H. M. Ramos, PAT design strategy for energy recovery in water distribution networks by electrical regulation, Energies 6 (1) (2013) 411–424. doi:10.3390/en6010411.

[7] A. Carravetta, G. Del Giudice, O. Fecarotta, H. M. Ramos, Pump as turbine (PAT) design in water distribution network by system effectiveness, Water 5 (3) (2013) 1211–1225. doi:10.3390/w5031211.

[8] A. Carravetta, O. Fecarotta, H. Ramos, A new low-cost installation scheme of PATs for pico-hydropower to recover energy in residential areas, Renewable Energy 125 (2018) 1003 – 1014. doi:10.1016/j.renene.2018.02.132.

[9] B. Capelo, M. Pérez-Sánchez, J. F. Fernandes, H. M. Ramos, P. A. López-Jiménez, P. C. Branco, Electrical behaviour of the pump working as turbine in off grid operation, Applied Energy 208 (2017) 302–311. doi:10.1016/j.apenergy.2017.10.039.

[10] S. Derakhshan, A. Nourbakhsh, Experimental study of characteristic curves of centrifugal pumps working as turbines in different specific speeds, Experimental Thermal and Fluid Science 32 (3) (2008) 800–807. doi:10.1016/j.expthermflusci.2007.10.004.

[11] F. Pugliese, F. De Paola, N. Fontana, M. Giugni, G. Marini, Experimental characterization of two pumps as turbines for hydropower generation, Renewable Energy 99 (2016) 180–187, doi:10.1016/j.renene.2016.06.051.

[12] S. Barbarelli, M. Amelio, G. Florio, Experimental activity at test rig validating correlations to select pumps running as turbines in microhydro plants, Energy Conversion and Management 149 (2017) 781 – 797, doi: 10.1016/j.enconman.2017.03.013.

[13] P. Kundur, N. J. Balu, M. G. Lauby, Power system stability and control, Vol. 7, McGraw-hill New York, 1994.

[14] G. A. Munoz-Hernandez, D. I. Jones, et al., Modelling and controlling hydropower plants, Springer, 2012. doi:10.1007/978-1-4471-2291-3.

[15] L. Belhadji, S. Bacha, I. Munteanu, A. Rumeau, D. Roye, Adaptive MPPT applied to variable-speed microhydropower plant, IEEE Transactions on Energy Conversion 28 (1) (2013) 34–43. doi:10.1109/TEC.2012.2220776.

[16] M. G. Molina, M. Pacas, Improved power conditioning system of micro-hydro power plant for distributed generation applications, in: 2010 IEEE Int. Conf. Industrial Technology (ICIT), pp. 1733–1738. doi:10.1109/ICIT.2010.5472461.

[17] J. Márquez, M. Molina, J. Pacas, Dynamic modeling, simulation and control design of an advanced micro-hydro power plant for distributed generation applications, International Journal of Hydrogen Energy 35 (11) (2010) 5772–5777. doi:10.1016/j.ijhydene.2010.02.100.

[18] Y. Pannatier, B. Kawkabani, C. Nicolet, J.-J. Simond, A. Schwery, P. Allenbach, Investigation of control strategies for variable-speed pump-turbine units by using a simplified model of the converters, IEEE Transactions on Industrial Electronics 57 (9) (2010) 3039–3049. doi:10.1109/TIE.2009.2037101.

[19] J. I. Sarasúa, J. I. Pérez-Díaz, J. R. Wilhelmi, J. Á. Sánchez-Fernández, Dynamic response and governor tuning of a long penstock pumped-storage hydropower plant equipped with a pump-turbine and a doubly fed induction generator, Energy Conversion and Management 106 (2015) 151–164. doi:10.1016/j.enconman.2015.09.030.

[20] C. Moreira, N. Fulgêncio, B. Silva, C. Nicolet, A. Béguin, Identification of dynamic simulation models for variable speed pumped storage power plants, Journal of Physics: Conference Series 813 (2017) 012006. doi:10.1088/1742-6596/813/1/012006.

[21] A. Béguin, C. Nicolet, J. Hell, C. Moreira, Assessment of power step performances of variable speed pump-turbine unit by means of hydro-electrical system simulation, Journal of Physics: Conference Series 813 (2017) 012001. doi:10.1088/1742-6596/813/1/012001.

[22] H. Ramos, A. Almeida, Dynamic orifice model on waterhammer analysis of high or medium heads of small hydropower schemes, Journal of Hydraulic Research 39 (4) (2001) 429–436. doi:10.1080/00221680109499847.

[23] H. Ramos, A. Betâ mio de Almeida, Parametric analysis of water-hammer effects in small hydro schemes, Journal of Hydraulic Engineering 128 (7) (2002) 689–696. doi:10.1061/(ASCE)0733-9429(2002)128:7(689).

[24] M. H. Chaudhry, Applied hydraulic transients, Springer, 1979. doi:10.1007/978-1-4614-8538-4.

[25] E. De Jaeger, N. Janssens, B. Malfliet, F. Van De Meulebroeke, Hydro turbine model for system dynamic studies, IEEE Transactions on Power Systems 9 (4) (1994) 1709–1715. doi:10.1109/59.331421.

[26] Working Group on Prime Mover and Energy Supply Models for System Dynamic Performance Studies, Hydraulic turbine and turbine control models for system dynamic studies, IEEE Transactions on Power Systems 7 (1) (1992) 167–179. doi:10.1109/59.141700.

[27] J.-K. Lung, Y. Lu, W.-L. Hung, W.-S. Kao, Modeling and dynamic simulations of doubly fed adjustable-speed pumped storage units, IEEE Transactions on Energy Conversion 22 (2) (2007) 250–258. doi:10.1109/TEC.2006.875481.

[28] M. Pérez-Sánchez, P. A. López-Jiménez, H. M. Ramos, Modified affinity laws in hydraulic machines towards the best efficiency line, Water Resources Management (2018) 1–16doi:10.1007/s11269-017-1841-0.

[29] M. P. Kazmierkowski, L. G. Franquelo, J. Rodriguez, M. A. Perez, J. I. Leon, High-performance motor drives, IEEE Industrial Electronics Magazine 5 (3) (2011) 6–26. doi:10.1109/MIE.2011.942173.

[30] D. P. Wadduwage, C. Q. Wu, U. Annakkage, Power system transient stability analysis via the concept of lyapunov exponents, Electric Power Systems Research 104 (2013) 183 – 192. doi:10.1016/j.epsr.2013.06.011.

[31] H. Khalil, Nonlinear Systems, Pearson Education, Prentice Hall, 2002.